HEPCAT Year 1 Progress Report

Student: Ryan Milton (UCR); Advisor: Prof. M. Arratia (UCR); Lab Mentor: Dr. B. Nachman (SLAC)

I. INTRODUCTION

SiPM-on-tile calorimeters are a fundamental part of future collider detectors. This SiPM-on-tile technology uses small scintillating cells, each individually read out by a silicon photomultiplier (SiPM), facilitating a higher granularity in calorimeters. With a higher granularity, showers that develop within the calorimeter can be measured with fine detail and can be reconstructed precisely. These calorimeters have already been well-developed by the CALICE collaboration [1] and will be used in future detectors such as the CMS HGCAL at the High-Luminosity LHC [2]. The UCR group has designed a pair of SiPM-on-tile calorimeters for the ePIC experiment at the future Electon-Ion Collider — the insert [3] and the Zero-Degree Calorimeter (ZDC) [4]. We developed a graph neural network (GNN) based method that utilizes the high-granularity of the detectors to improve the reconstruction of showers in the calorimeters [5]. We have optimized the designs of these detectors in a differential way where we adjust a design specification and see how that impacts the GNN reconstruction, ultimately using the GNN performance to decide on the design of our detectors. In this report, we present our studies of using GNNs to reconstruct the Λ^0 from after detecting its neutral-channel decay products, $\Lambda^0 \to n\pi^0$, with the ZDC [6] and using GNNs to optimize the readout for the insert.

II. Λ^0-DECAY IN THE ZERO-DEGREE CALORIMETER

The ePIC Zero-Degree Calorimeter (ZDC), illustrated in Fig. 1, is essential for detecting neutral particles deflected at small angles. In our original design paper [4], we used a high-granularity design that improved reconstruction of simulated single and multiple neutrons that hit the ZDC. We also found that the angular resolution improved when we used a staggered readout for the ZDC, where the cells within each of the ZDC's layers are offset from the preceding and succeeding layers [7]. To test the ZDC's ability to reconstruct more complicated events, we simulated neutral Λ^0-decay events in the ZDC. According to the report on the science requirements and detector concepts for the EIC (EIC Yellow Report [8]), "The reconstruction of the Λ^0 event in the far-forward detection area is one of the most challenging tasks. This comes mainly from the fact that these leading Λ^0's have energy close to the initial beam energy, and thus their decay lengths can be tens of meters along the Z-axis (or beam-line)". An illustration of the neutral Λ^0-decay is shown in Fig. 2. Due to the π^0 's prompt decay to two photons, adequate reconstruction of the Λ^0 demands disentangling three separate particle showers. As shown in Fig. 3, this is difficult due to the complicated shower shapes in the ZDC, necessitating the high granularity of the detector. On top of this, the electromagnetic and hadronic components of the showers produce different responses within the ZDC and their energy dispositions need to be weighted with respect to one another to precisely reconstruct the energy of the Λ^0. While this can be done algorithmically through reweighting procedures, such as those developed by the CALICE collaboration [9], they take years to develop and optimize.

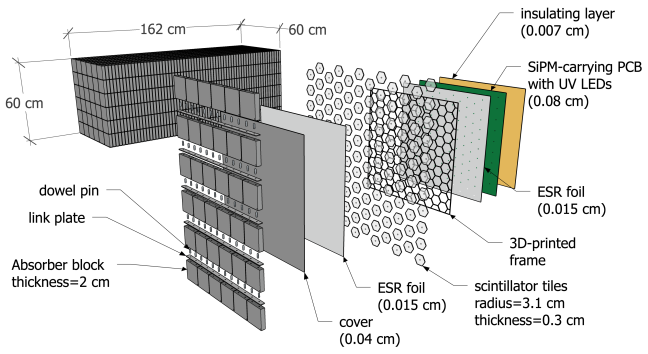

FIG. 1. The overall ZDC with one of its layers exploded. Figure reproduced from [4].

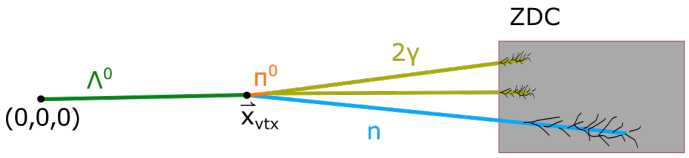

FIG. 2. An illustration of the neutral Λ^0-decay, $\Lambda^0 \to n\pi^0$. The Λ^0 is produced at the interaction point $(0,0,0)$ and travels to $\vec{x}_{\rm vtx}$ before decaying to a neutron and a π^0 (which promptly decays to two photons). The final state particles are detected within the ZDC. Figure reproduced from [6].

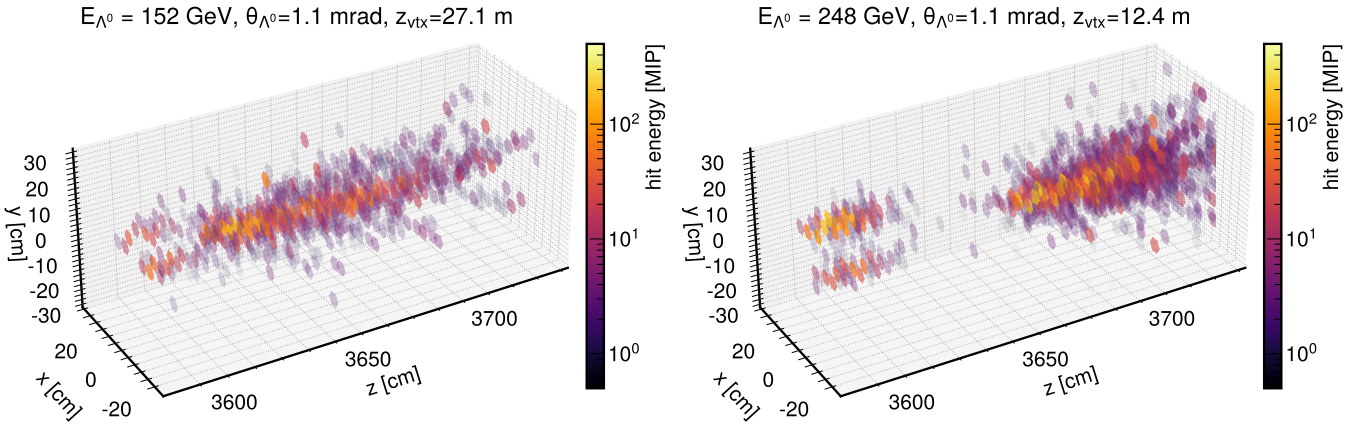

FIG. 3. Event displays of the Λ^0 decay products striking the ZDC. E_{Λ^0}, θ_{Λ^0}, and $z_{\rm vtx}$ in the titles are the Λ^0's generated energy, Λ^0's generated polar angle, and the z-distance the Λ^0 travels before decaying, respectively. The color scale represents the hit energy in units of the energy deposited by a minimum-ionizing particle (MIPs), which is 0.47 MeV. Figures reproduced from [6].

To best reconstruct the Λ^0, we use a graph neural network (GNN) approach. The showers in an event are represented as a graph, where the nodes are the detector cell energies and positions and they are connected to nearby cells with edges. The GNN takes these graphs and outputs the energy, polar angle, and azimuthal angle of the original Λ^0 particle. The full details of the GNN implementation can be found in References [4–6]. We previously tested and refined this GNN approach for the ZDC using simpler events with single and multiple neutrons [4]. In this neutron study, the GNN method improved the ZDC's energy and angular resolution compared to by-hand reweighting methods. The main results from the Λ^0 studies are shown in Fig. 4. We again see improvements in the reconstruction of the energy and angles of the Λ^0 using GNNs compared to other reweighting methods. We also trained a GNN classifier to differentiate between Λ^0 and single neutron events. We found that while just 4%-8% of events are correctly identified as Λ^0 with conventional reconstruction, 43%-70% events are correctly identified by the GNN (the range in identification efficiency is due to measuring at various energies). Both methods misidentify less than 1% of single neutron events.

With the GNN reconstruction of single neutrons in previous studies and the Λ^0 in these studies, we have motivated the ZDC design with high-granularity readouts and staggered layers. Moreover, despite there being electromagnetic showers in the Λ^0 events, the high-granularity ZDC alone can reconstruct the Λ^0. This supports the idea that an electromagnetic calorimeter may not be needed in front of the ZDC during experimental operation for reactions like the Λ^0-decay.

III. INSERT SEGMENTATION

The ePIC insert is a SiPM-on-tile sampling calorimeter (layers of 1.6 cm steel, 0.3 cm scintillator) that extends the range of pseudorapidity covered in the hadron-going direction of the experiment. The detector surrounds the beampipe, as shown in Fig. 5, and is designed similarly to the ZDC. A key purpose of this detector is to measure high-energy jets that would otherwise go undetected in the absence of the detector. In this study, we attempt to quantify the performance difference of two insert configurations.

The first configuration, displayed in Fig. 6, is referred to as the "high-granularity insert". This version has 16 layers

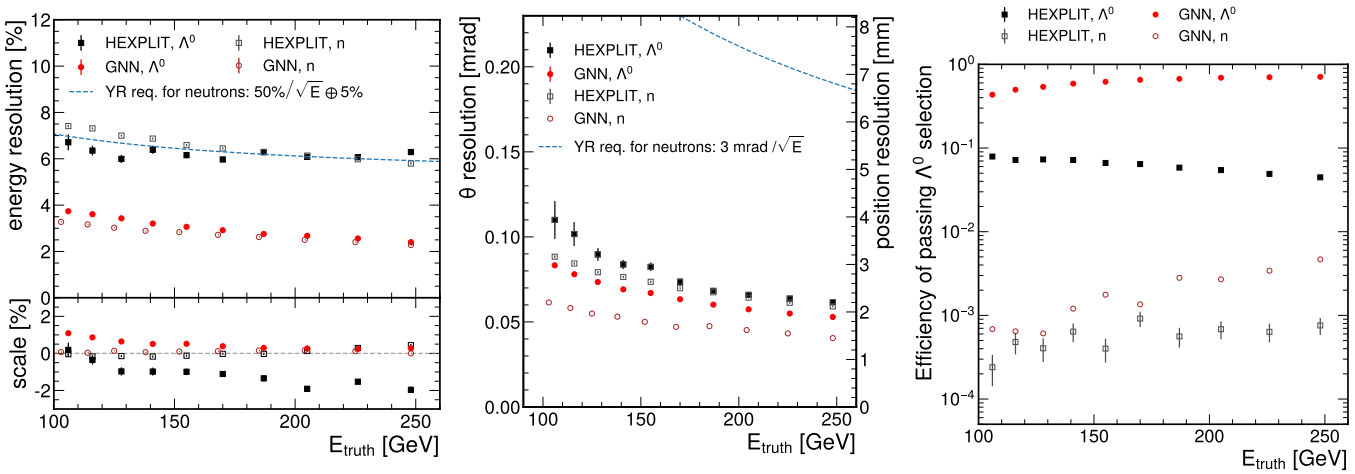

FIG. 4. Results from the Λ^0-decay studies. The left panel shows the energy resolution and the scale. The scale is the mean value of $(E^{\Lambda^0}_{rec} - E^{\Lambda^0}_{truth})/E^{\Lambda^0}_{truth}$. The middle panel shows the resolution of the reconstructed polar angle and position of the Λ^0. The right panel shows the fraction of Λ^0 events classified as Λ^0 (solid points) and single neutron events misclassified as Λ^0 events (open points). These results are compared to results from using HEXPLIT, a subcell energy reweighting method [7]. The results for the energy and angular/position resolutions satisfy the requirements set by the EIC Yellow Report [8]. Figures reproduced from [6].

of staggered 14 cm^2 hexagonal cells, followed by 44 layers of unstaggered 21 cm^2 hexagonal cells (left side) and 25 cm^2 hexagonal cells (right side). Each cell in this configuration is read out individually. One main motivation for this high-granularity version is the ability to separate the multiple showers from the jets and other particles. The second configuration, referred to as the "low-granularity insert" has 60 layers of unstaggered 25 cm^2 square cells, with the readout integrated longitudinally into 7 segments (layers 1-12, 13-20, 21-28, 29-36, 37-44, 45-52, and 43-60). This version has about 25% fewer total cells and hence silicon photomultipliers. Note that the insert has an electromagnetic calorimeter in it, making the scenario different than the ZDC studies.

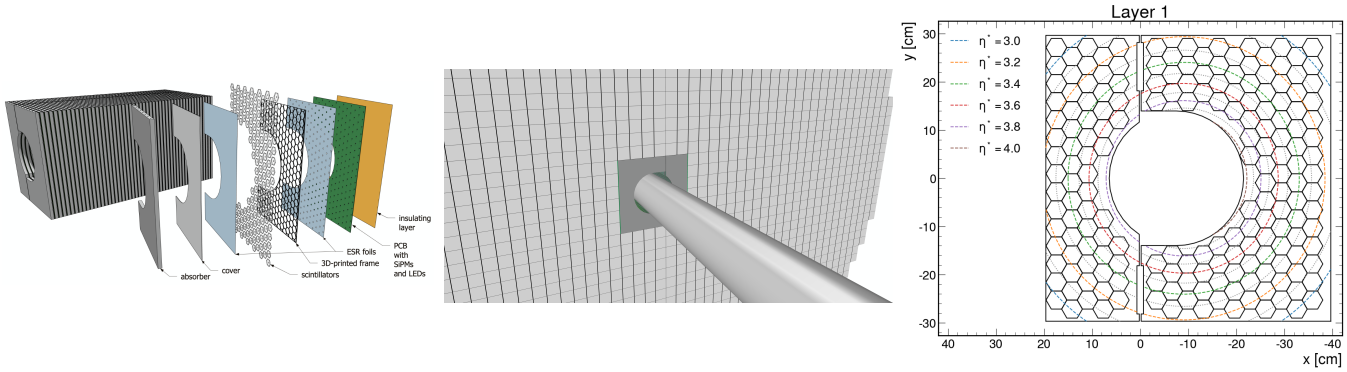

FIG. 5. Design of the insert. The left panel shows the layers of the insert, which is split with each half on either side of the beampipe. The middle panel shows the insert (dark gray) surrounding the beampipe. The light gray squares are a larger, surrounding hadronic calorimeter. The right panel displays the ranges of psuedorapidity covered by the insert. The pseudorapidity η^* is marked with an asterisk to denote it is calculated with respect to the proton axis. These figures use hexagonal cells, similar to the high-granularity insert, for illustration purposes. Figures reproduced from [3] (right figure is a modified figure).

To gauge the performance of the two configurations, we used simulations of single neutron and of $\rho^0 \to \pi^+\pi^-$, the latter of which is a proxy for multi-shower performance. We again use the GNN approach to predict the energies and angles of the particles given the energies and positions of the cells of both the electromagnetic calorimeter and the insert.

The energy and angular resolutions for the neutron simulations are shown in Fig. 7. We see similar energy and ϕ resolutions, whereas the θ resolution is about 5% better for the high-granularity configuration. The similarity in energy resolution is not unexpected since the total energy deposition in the two detectors is similar. We see a worse

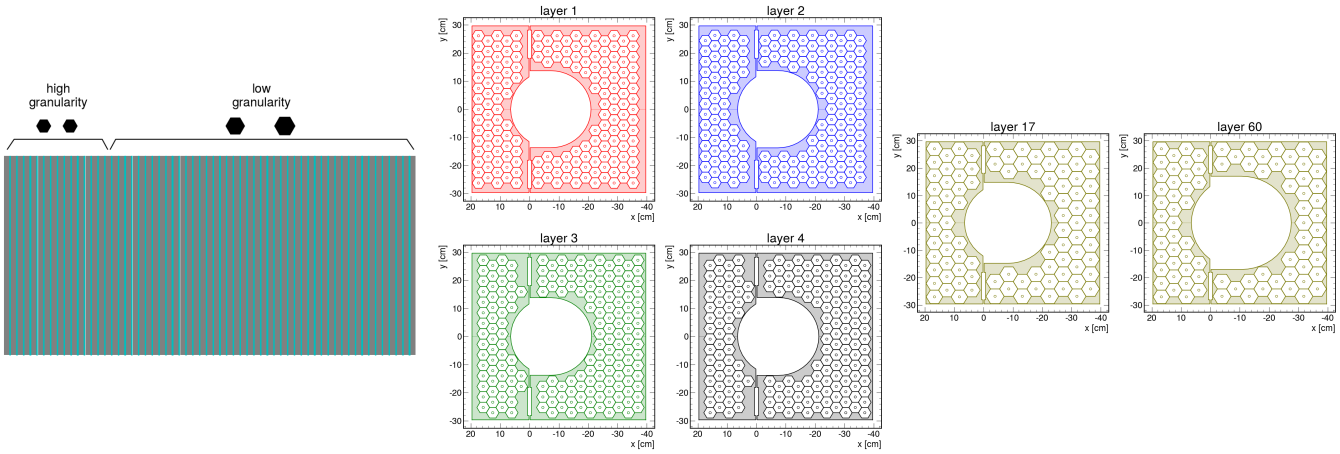

FIG. 6. Design of the high-granularity insert. The left panel shows the higher granularity and lower granularity sections of the detector. The middle panel shows the cell layout in the first 16 layers. Note that the cells are staggered (they alternate positions) between layers. The right panel shows the unstaggered cells in the final 44 layers.

performance in the $3.8 < \eta^* < 4$ bin, which is the area closest to the beampipe where showers are likely less well contained. Note that these results are different than what we observed in our previous study on segmentation [5], where we saw that increasing the amount of segmentation improved our energy resolutions. This study was done with the DeepSets neural network model though, while graph neural networks are used here. DeepSets does not connect nearby cells together, which seems to cause a difference in results.

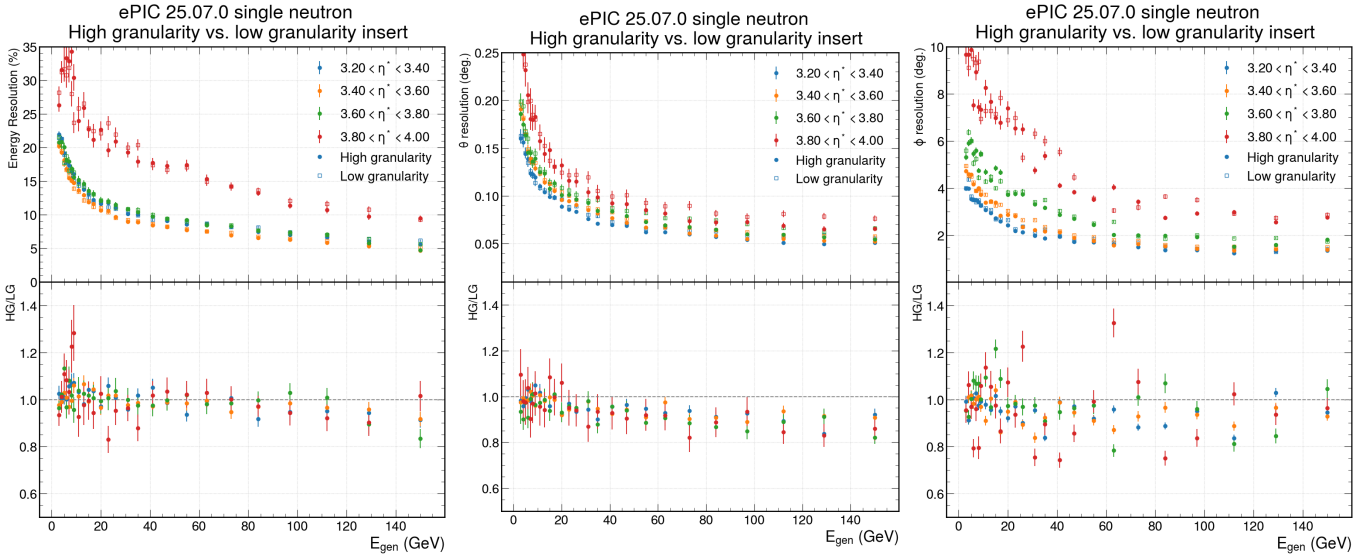

FIG. 7. Resolutions from single-neutron simulations of energy (left), θ (middle), and ϕ (right). The bottom panels give the ratio of the high-granularity resolution to low-granularity resolution in each bin.

The ρ^0-decay events, shown in Fig. 8 are more complicated due to multiple showers. Instead of predicting the ρ^0 energy and angles, the GNN predicts the energy and angles of each pion from the decay. To quantify the performance, we obtain the resolution for each pion separately and sum the resolutions in quadrature. We do this in bins of energy and asymmetry, $(E_{\text{high}} - E_{\text{low}})/(E_{\text{high}} + E_{\text{low}})$, where E_{high} (E_{low}) is the energy of the higher (lower) energy pion in the event. This quantity relates to the angular separation of the two particles. The performance is shown in Fig. 9. Again, we see similar results between the two configurations.

We also tried training a GNN where we only give the network the insert hits without the hits from the electromagnetic calorimeter. The overall results are worse due to the GNN having less shower information. Interestingly though, the two configurations show a large difference, with the high-granularity configuration having 20% better resolutions.

These studies are still being finalized, but we again show that GNNs are a powerful tool that we are using to

improve calorimeter resolutions and motivate detector design choices. Note that these results are not trivial. We had an expectation that the high-granularity configuration might improve reconstruction, but it is difficult to quantify this. As mentioned previously, developing a sophisticated reconstruction algorithm takes many years to develop, as seen in the CALICE studies [9]. This CALICE algorithm was developed for a single detector. In this study, we used a mature reconstruction method for multiple detectors with very different energy deposition patterns, as well as different types of reactions. Developing proper reweighting procedures for this study would be difficult and time-consuming. These types of studies were only feasible with our AI/ML reconstruction techniques.

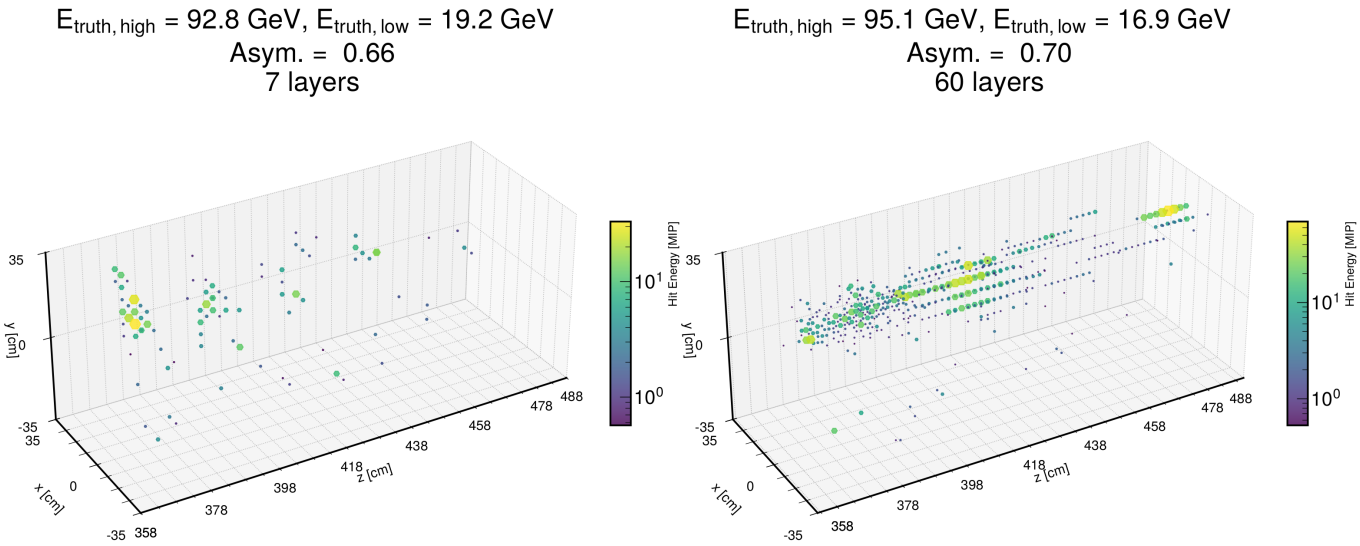

FIG. 8. Event displays of the ρ^0 decay products striking the insert. The left figure (labeled 7 layers) is the low-granularity configuration and the right figure (labeled 60 layers) is the high-granularity configuration. $E_{\text{truth,high}}$ and $E_{\text{truth,low}}$ are the energies of the higher energy and lower energy pions in the event, respectively. The asymmetry is also denoted. The color scale represents the hit energy in units of the energy deposited by a minimum-ionizing particle (MIPs), which is 0.47 MeV.

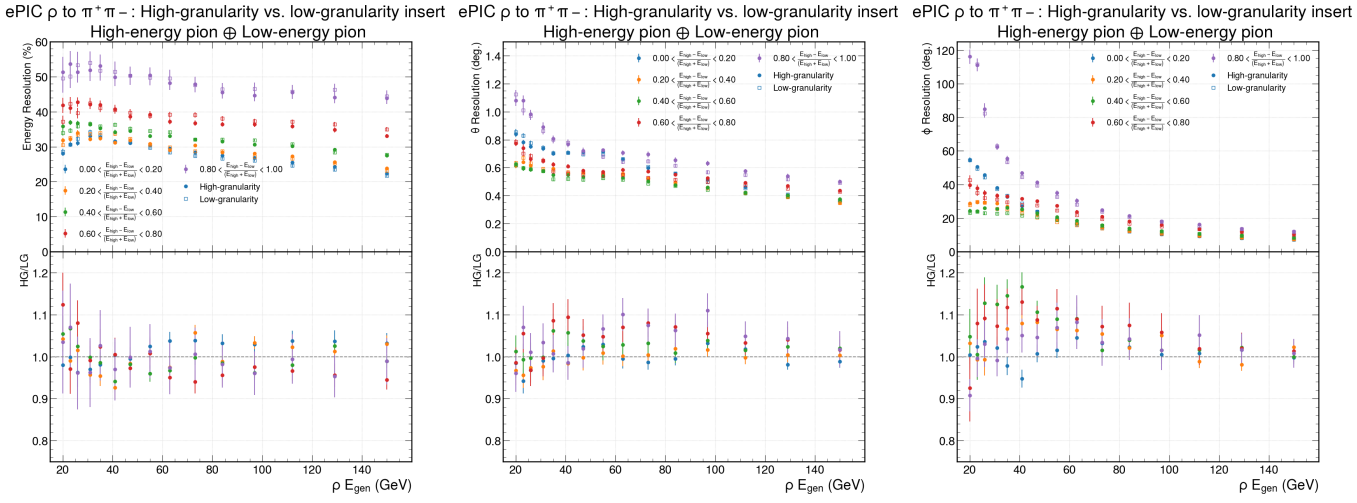

FIG. 9. Resolutions from ρ^0 simulations of energy (left), θ (middle), and ϕ (right). The bottom panels give the ratio of the high-granularity resolution to low-granularity resolution in each bin. The GNN outputs predictions for each decay pion separately, so we sum the resolutions for each pion in quadrature. We bin in terms of energy and asymmetry.

IV. PLANS FOR YEAR 2

In the second year of the HEPCAT project, our main aim is to refine our GNN studies and deploy them to data from beam tests.

The first task is to finalize the insert segmentation studies. We saw in our previous studies that training a GNN with data from a high-granularity configuration and low-granularity configuration produce similar energy and angular resolutions. However when the GNN is only trained on the insert hits without the electromagnetic hits, there is a 20% difference between the two. This suggests that events with little energy in the electromagnetic calorimeter may look different when using the two configurations. These types of events may motivate the high-granularity design over the low-granularity design. We will iterate on these studies and choose the final optimized design, determined through GNNs. Additionally, we will use our GNN studies of the ZDC and the insert in the ePIC Technical Design Report to motivate their designs.

Over the past two years, the UCR group has performed beam tests at Brookhaven National Lab [10], Jefferson Lab [11], and the Crocker Nuclear Laboratory at UC Davis [12] using prototypes of the insert and the ZDC. Pictures from the beam tests are shown in Fig. 10 We will use the results of these beam tests to make the detector simulations more realistic to better match the taken data. In these tests, we also studied the impact of radiation damage on the detectors' SiPMs and the crosstalk between channels. We will use these studies to implement a realistic noise model into our simulations and develop a noise-resistant reconstruction method with GNNs. We will perform more beam tests over the next year where we will deploy our GNN-methods. Ryan will be directly involved in the data-taking and analysis of the beam test data. We will make a realistic simulation of the detector and match the simulated signals to the data, incorporating findings from previous studies like crosstalk. Once the simulation is validated against the test beam, use the simulated data to train a GNN and use it to predict event properties using real data. This will be the first time we have used our AI/ML models on non-simulated data, and will represent a key step in validating our GNN-based reconstruction method.

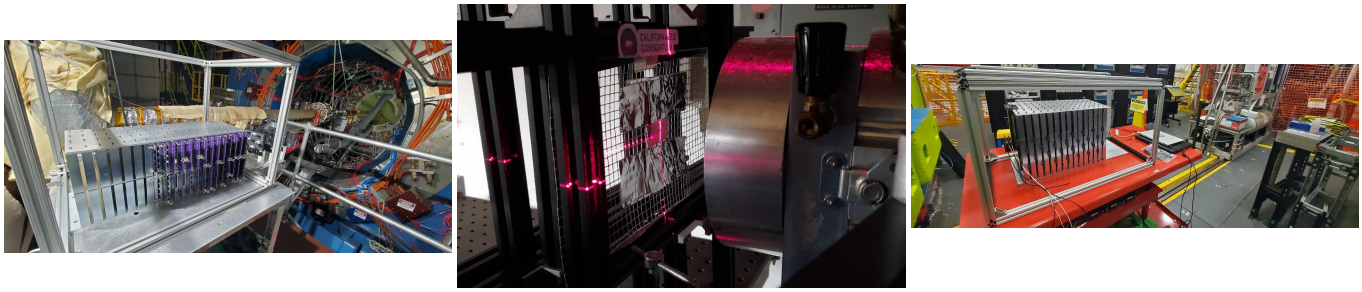

FIG. 10. Photos from previous beam tests. The left figure shows an insert prototype in the STAR hall where it took data parasitically during STAR runs (original image from [10]). The middle photo was taken at a SiPM-irradiation test at the UC Davis Cyclotron, with a SiPM mounted in front of the cyclotron beam (original image from [12]). The right photo is shows our latest ZDC prototype in Hall D at Jefferson Lab (paper not yet released, photon given courtesy of Sean Preins from UCR).

REFERENCES

[1] A. White *et al.* (CALICE), Design, construction and commissioning of a technological prototype of a highly granular SiPM-on-tile scintillator-steel hadronic calorimeter, JINST **18** (11), P11018, arXiv:2209.15327 [physics.ins-det].

[2] The Phase-2 Upgrade of the CMS Endcap Calorimeter 10.17181/CERN.IV8M.1JY2 (2017).

[3] M. Arratia *et al.*, A high-granularity calorimeter insert based on SiPM-on-tile technology at the future Electron-Ion Collider, Nucl. Instrum. Meth. A **1047**, 167866 (2023), arXiv:2208.05472 [physics.ins-det].

[4] R. Milton, S. J. Paul, B. Schmookler, M. Arratia, P. Karande, A. Angerami, F. T. Acosta, and B. Nachman, Design and simulation of a SiPM-on-tile ZDC for the future EIC, and its performance with graph neural networks, Nucl. Instrum. Meth. A **1079**, 170613 (2025), arXiv:2406.12877 [physics.ins-det].

[5] F. T. Acosta, B. Karki, P. Karande, A. Angerami, M. Arratia, K. Barish, R. Milton, S. Morán, B. Nachman, and A. Sinha, The optimal use of segmentation for sampling calorimeters, JINST **19** (06), P06002, arXiv:2310.04442 [physics.ins-det].

[6] S. J. Paul, R. Milton, S. Morán, B. Schmookler, and M. Arratia, Feasibility study of measuring $\Lambda 0 \to n\pi 0$ using a high-granularity zero-degree calorimeter at the future electron-ion collider, Phys. Rev. D **111**, 092013 (2025), arXiv:2412.12346 [nucl-ex].

[7] S. J. Paul and M. Arratia, Leveraging staggered tessellation for enhanced spatial resolution in high-granularity calorimeters, Nucl. Instrum. Meth. A **1060**, 169044 (2024), arXiv:2308.06939 [physics.ins-det].

[8] R. Abdul Khalek *et al.*, Science Requirements and Detector Concepts for the Electron-Ion Collider: EIC Yellow Report, Nucl. Phys. A **1026**, 122447 (2022), arXiv:2103.05419 [physics.ins-det].

[9] C. Adloff *et al.* (CALICE), Hadronic energy resolution of a highly granular scintillator-steel hadron calorimeter using software compensation techniques, JINST **7**, P09017, arXiv:1207.4210 [physics.ins-det].

[10] W. Zhang, S. Preins, J. Huang, S. J. Paul, R. Milton, M. Rodriguez, P. Carney, R. Tsiao, Y. Abdelkadous, and M. Arratia, First-ever deployment of a SiPM-on-tile calorimeter in a collider: a parasitic test with 200 GeV p p collisions at RHIC, JINST **20** (06), P06029, arXiv:2501.08586 [physics.ins-det].

[11] M. Arratia, B. Bagby, P. Carney, J. Huang, R. Milton, S. J. Paul, S. Preins, M. Rodriguez, and W. Zhang, Beam Test of the First Prototype of SiPM-on-Tile Calorimeter Insert for the EIC Using 4 GeV Positrons at Jefferson Laboratory, Instruments **7**, 43 (2023), arXiv:2309.00818 [physics.ins-det].

[12] J. Huang, S. Preins, R. Tsiao, M. Rodriguez, B. Schmookler, and M. Arratia, Measurement of SiPM Dark Currents and Annealing Recovery for Fluences Expected in ePIC Calorimeters at the Electron-Ion Collider, (2025), arXiv:2503.14622 [physics.ins-det].